

Active Tension Network model reveals an exotic mechanical state realized in epithelial tissues

Nicholas Noll,¹ Madhav Mani,^{2,3} Idse Heemskerk,^{4,3}

Sebastian Streichan,³ and Boris I. Shraiman^{1,3}

¹*Department of Physics, University of California Santa Barbara*

²*Department of Applied Mathematics, Northwestern University*

³*Kavli Institute for Theoretical Physics*

⁴*Department of Biosciences, Rice University*

Abstract

Mechanical interactions play a crucial role in epithelial morphogenesis, yet understanding the complex mechanisms through which stress and deformation affect cell behavior remains an open problem. Here we formulate and analyze the Active Tension Network (ATN) model, which assumes that mechanical balance of cells is dominated by cortical tension and introduces tension dependent active remodeling of the cortex. We find that ATNs exhibit unusual mechanical properties: i) ATN behaves as a fluid at short times, but at long times it supports external tension, like a solid; ii) its mechanical equilibrium state has extensive degeneracy associated with a discrete conformal - “isogonal” - deformation of cells. ATN model predicts a constraint on equilibrium cell geometry, which we demonstrate to hold in certain epithelial tissues. We further show that isogonal modes are observed in a fruit fly embryo, accounting for the striking variability of apical area of ventral cells and helping understand the early phase of gastrulation. Living matter realizes new and exotic mechanical states, understanding which helps understand biological phenomena.

Mechanics of growth and cellular rearrangements plays an important role in morphogenesis as both processes are central to defining the shape of developing tissues. As such, it has become a subject of intense study aiming to characterize specific mechanical processes involved in cell and tissue-wide dynamics[1–4], uncover the regulatory mechanisms [5], and identify if and how the mechanical state of the cell feeds back onto the larger developmental program [6–8].

Epithelial tissue is a monolayer of apico-basally polarized cells tightly connected to their lateral neighbors [9]. Viewed from the apical side, cells form an approximately polygonal tiling of the plane. Mechanical integrity of the epithelial layer derives largely from the cortical actin-myosin network [10, 11] localized as a planar ring just inside the cell’s lateral surface [12]. Each cell’s cortical cytoskeleton is linked to those of the neighboring cells via cadherin-mediated adherens junctions [13]. The equilibrium geometry of cells is determined by the balance of cytoskeletal and adhesive forces [5] within the tissue. Unlike passive materials, cells actively regulate such forces through mechano-transduction and internal remodeling, resulting in an intrinsically dynamic relation of stress and strain and controllable plasticity [14, 15], which can drive rearrangement of cells. Elucidation of the manner in which cellular activity manifests in collective properties of the tissue is critical to understanding morphogenesis.

Here we formulate a phenomenological model of an epithelial tissue as a two dimensional Active Tension Network (ATN), which in addition to cytoskeletal elasticity describes cytoskeletal re-arrangement through myosin activity and the recruitment of myosin into cytoskeletal fibers, thus capturing the plastic and adaptive response of cells to external stress. We shall explore static and dynamic properties of the ATN model, validate some of its predictions by comparing with experimental observations and identify new directions of further study.

Formulation of the Active Tension Net Model

Epithelial monolayers may be approximately represented by two-dimensional polygonal tilings, parameterized by the set of vertex coordinates $\{\mathbf{r}_i\}$ and are often described in terms

by vertex models [2, 17] which assume that geometry of cells minimizes an elastic energy defined in terms of cell edge length ($r_{ij} = |\mathbf{r}_i - \mathbf{r}_j|$) and cell area (A_α). We shall introduce a generalized class of vertex models by adding internal variables to capture active adaptation of the cytoskeleton. We begin by defining mechanical energy in its differential form [16]

$$dE[\{\mathbf{r}_i\}] = \sum_{\langle i,j \rangle} T_{ij} dr_{ij} + \sum_{\alpha} p_{\alpha} dA_{\alpha} \quad (1)$$

Here tension T_{ij} defines the change in mechanical energy in response to the change of edge length by dr_{ij} and 2D ‘apical pressure’ p_{α} defines the response to the change in cortical area by dA_{α} . Tension Nets correspond to the situation when pressure differentials between cells are small so that mechanical balance is dominated by the tensions, in which case $p_{\alpha} \approx p_0$ with p_0 effectively controlling only the total area of cells and preventing the collapse of the array under the action of tension.

Dynamics of vertex positions is assumed to be relaxational and in the Tension Net approximation becomes

$$\nu \frac{d}{dt} \mathbf{r}_i = -\partial_{\mathbf{r}_i} E = \sum_{\{j\}_i} T_{ij} \hat{\mathbf{r}}_{ij} \quad (2)$$

where $\{j\}_i$ denotes the set of all vertices connected to vertex i , $\hat{\mathbf{r}}_{ij}$ is a unit vector in the direction from \mathbf{r}_i to \mathbf{r}_j and ν represents the effective friction between apical cytoskeleton and its substrate [18], which sets the timescale of mechanical relaxation. Mechanical equilibrium of a Tension Net is reached when tensions balance at each vertex: the right hand side of Eq. (2) is zero. Geometrically this corresponds to the three vectors $\mathbf{T}_{ij} = T_{ij} \hat{\mathbf{r}}_{ij}$ making up a triangle and since adjacent vertices share an edge, global tension balance means that the set of T_{ij} ’s defines a triangulation [27, 28] (see Fig. 1a,b).

Edge tension T_{ij} depends on the edge length r_{ij} and intrinsic variables representing local state of the actomyosin bundle and cadherin mediated adhesion between cells. We shall start with a particularly simple form, $T_{ij} = k(r_{ij} - \ell_{ij})$, parameterizing the internal state of the each interface by an intrinsic ‘rest length’ ℓ_{ij} of the underlying actomyosin bundle. The latter has dynamics of its own. Specifically, we shall assume that

$$\ell_{ij}^{-1} \frac{d}{dt} \ell_{ij} = \tau_{\ell}^{-1} W \left(\frac{T_{ij}}{m_{ij} a T_s} \right) \quad (3)$$

The generic features of "walking kernel" $W(x)$, illustrated in Fig.1d, are known from single-molecule experiments [19, 20]: each myosin will walk contracting the actin bundle, unless the load per myosin, T_{ij}/am_{ij} , reaches the "stall force" level T_s . (The characteristic length a describes the extent to which myosin motors share mechanical load.) Above this critical value, the filament simply elongates as each motor slips backwards [21].

Eqs. (2, 3) define the dynamics of a Tension Net with a specified myosin distribution on interfaces. The fixed point of these equations is then reached when i) tensions balance at all vertices and ii) all edges are at their stall tension, set by the local myosin level ($T_{ij} = aT_s m_{ij}$). Because tension balance requires the set of T_{ij} 's to form a triangulation, edge tensions, and hence myosin levels, cannot be prescribed independently. Luckily, in reality myosin levels are not fixed and are known to themselves respond to mechanical cues [8, 22], although the exact form of this mechanical feedback is not fully understood. Here we shall propose a particular form of mechanical feedback on myosin, that will ensure convergence to a balanced state. The latter is achieved if myosin recruitment depends on internal strain rate:

$$m_{ij}^{-1} \frac{d}{dt} m_{ij} = \alpha \ell_{ij}^{-1} \frac{d\ell_{ij}}{dt} = \alpha \tau_\ell^{-1} W \left(\frac{T_{ij}}{m_{ij} a T_s} \right) \quad (4)$$

with $\alpha \ll 1$ parameterizing the rate of myosin recruitment which we assume to be slow relative to both mechanical relaxation and actomyosin contractility. This "Dynamic Recruitment" form of mechanical feedback builds up myosin on overloaded and therefore "slipping" bundles and reduces myosin on underloaded and contracting bundles until the stall condition is reached, bringing the system to equilibrium. This hypothesis is dictated by the requirement of ATN stability and should be regarded as a prediction of the model, to be tested by future experiments.

Equilibrium Manifold of a Tension Net

Mechanical equilibrium a Tension Net requires a local balance of tensions (see Eq. (2)) which relates the geometry of the cell array to a triangulation of the "tension plane" (see Fig. 1). This relation involves the $\theta_{i\alpha}$ angles at vertex i which define angles of the i^{th} tension triangle with $\pi - \theta_{i\alpha}$ being the angle opposite of the T_{ij} side (see Fig.1). The fact that

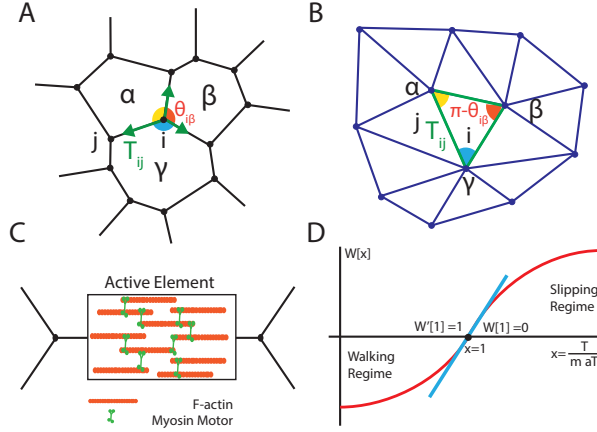


FIG. 1. (a) Tension Net representation of a 2D array of cells. In mechanical equilibrium tensions balance at each vertex; (b) Tensions corresponding to an equilibrium state form a triangulation, with triangle angles being supplementary to the angles at the corresponding vertex; (c) A cartoon representation of the actomyosin bundle as the active element of the cortical cytoskeleton (d) Dependence of the actomyosin bundle contraction rate to the mechanical load. The "walking kernel" $W(x)$, see Eq. (3), changes sign from contraction to elongation when mechanical load per myosin T/am exceed the stall load T_s .

triangles corresponding to vertices that belong to the the same cell pack together into a triangulation constrains the angles

$$\chi_\alpha = \prod_{i \in \mathcal{V}(\alpha)} \frac{\sin \theta_{i,\alpha}}{\sin \theta_{i-1,\alpha}} = 1 \quad (5)$$

where i labels the vertices of cell α , denoted as $\mathcal{V}(\alpha)$, in a clockwise fashion. This constraint follows directly from the sine law applied to the triangles that share vertex α of the triangulation. A polygonal array with all $\chi_\alpha = 1$ is geometrically *compatible* with tension balance equilibrium. Since χ_α can be readily computed for any polygonal array, the compatibility constraint allows one to asses whether a given cell array could be a balanced tension net.

To count the number of degrees of freedom that define balanced tension configurations we note that a triangulation is completely specified by the positions of its vertices, the number of which equals c - the number of polygonal cells - so that triangulation is specified by $2c$ independent degrees of freedom. Note that the number of edges $e = 3c$ is larger than $2c$

meaning that T_{ij} cannot be chosen independently; the balanced set of tensions satisfies c angular constraints imposed by the planarity of the triangulation.

Next we observe that the number of degrees of freedom for equilibrium tension net geometries, given by $2v - c = 3c$ (v being the number of vertices of the cell array), is larger than the $2c$ degrees of freedom for the dual triangulations of the tension plane. Hence, a given set of tensions must correspond to multiple possible cell arrays: specifically, to a manifold of nets with one degree of freedom per cell. Given a triangulation we can construct a dual polygonal lattice by defining the circumcircle center for each triangle and drawing a Voronoi lattice based on these centroids. Yet, such a lattice is not the unique dual of the tension triangulation. As long as none of the vertex angles are perturbed, we can freely “inflate” or “deflate” lattice cells, as illustrated in Fig. 2(a), with no cost of energy and thus without disturbing mechanical equilibrium and the underlying tension-triangulation. Quite generally such angle preserving - “isogonal” - deformations have the form

$$\delta \mathbf{r}_i = S_{\alpha\beta\gamma}^{-1} [\mathbf{T}_{ij}\Theta_\gamma + \mathbf{T}_{ik}\Theta_\alpha + \mathbf{T}_{il}\Theta_\beta] \quad (6)$$

where $\delta \mathbf{r}_i$ denotes displacement of vertex at which adjacent cells α, β, γ meet and $S_{\alpha\beta\gamma}$ (Fig. 1ab) denotes the area of said vertex’s dual triangular plaquette and Θ_α ’s are independent parameters. Tensions T_{ij} appear as coefficients because their ratios capture the implicit geometric constraints within tension nets central to the structure of the isogonal modes. (Note for example that $\delta \mathbf{r}_i = 0$ for $\Theta_\alpha = \Theta_\beta = \Theta_\gamma$.) The compatibility condition (see Eq. 5) satisfied by equilibrium tension nets is essential for allowing such isogonal dilation modes to exist! Because they do not invoke a restoring force, isogonal deformations are the easily excitable “soft modes” which are expected to dominate observed fluctuations of tension nets close to mechanical equilibrium.

We note also that isogonal modes can be thought of as a discrete manifestation of the conformal symmetry that appears in 2D continuum elasticity in the case of a vanishing bulk modulus (see SI for details). Isogonal modes also generalize the isoperimetric “breathing modes” of a hexagonal lattice [23].

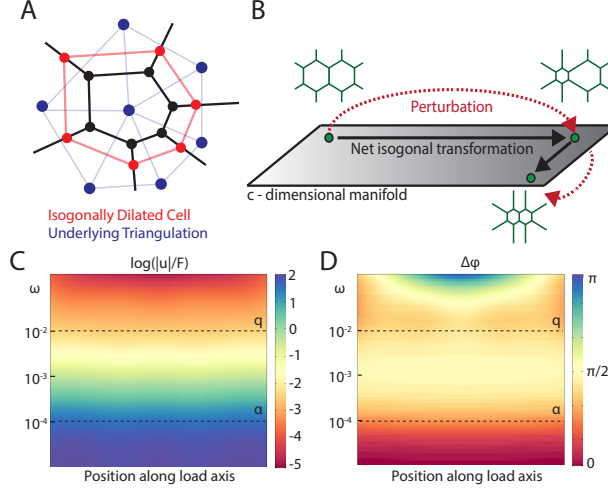


FIG. 2. (a) Cartoon illustrating the *isogonal*, i.e. angle preserving, ‘breathing mode’ of a cell in a tension net. (b) Because ATN equilibrium is a manifold rather than a point, after a transient perturbation the system does not necessarily return to the same state, resulting in an ‘isogonal’ transformation. (c) Amplitude and (d) phase of the strain (as a function of position in a 2D sheet) in response to periodic forcing $T_B \cos \omega t$ at the boundaries ($\alpha = 10^{-2}$ and $\omega = 10^{-4}$). As the frequency decreases below α the phase shifts from 0 to $\pi/2$ indicating crossover from viscous fluid behavior to an elastic solid. Crossover at $\omega \sim q$ corresponds to viscoelasticity.

Dynamical properties of Active Tension Nets.

Let us consider the dynamics of small perturbations around a mechanical equilibrium state, which can be described by linearizing Eqs. (2-4). While detailed calculations are carried out in the SI, the key features can be understood from a vastly simpler analysis of a 1D “active tension chain” model which has the form

$$\frac{d}{dt} \delta T_n = D \nabla^2 \delta T_n - q (\delta T_n - \delta m_n) \quad (7)$$

$$\frac{d}{dt} \delta m_n = \alpha (\delta T_n - \delta m_n) \quad (8)$$

where δT_n and δm_n are deviations from the equilibrium state, n -is an integer indexing the edges along the chain, ∇^2 is the discrete 1D Laplacian and D, q, α parameters are derived by linearization of Eqs. (2-4), see SI. The rate of strain in the chain is $\dot{u}_n = \frac{d}{dt} (r_{n+1} - r_n) =$

$\nu^{-1}\nabla^2\delta T_n$. With that, Eq. 7 is recognized as the Maxwell model of viscoelasticity forced by myosin. With a constant δm forcing these would predict persistent flow (i.e. non-zero rate of strain), perturbations of tension being exponentially localized with characteristic “screening length” $\lambda = \sqrt{D/q}$. At long times myosin recruitment (with $\alpha \ll q$) is important and the chain converges towards mechanical equilibrium: $\delta m_n \approx \delta T_n - q^{-1}D\nabla^2 T_n$ so that $\frac{d}{dt}\delta m_n \approx \alpha q^{-1}D\nabla^2 T_n$ and $\frac{d}{dt}T_n \approx \alpha D\nu^{-1}q^{-1}\dot{u}_n$ (see SI) This means that unlike viscoelastic flow response at short time, the long time behavior is effectively elastic with $k_{eff} \sim \alpha\nu^{-1}q^{-1}D$. A similar crossover from fluid-like response at intermediate time to solid-like behavior at long times occurs in the fully 2D ATN (see Fig. 2cd).

ATN predictions and the Ventral Furrow (VF) formation in *Drosophila* embryo.

One of the striking predictions of the ATN model is the existence of the isogonal soft modes that allow easy variability of cell area. Extreme variability of apical cell area has in fact been observed in the beginning of the gastrulation process in *Drosophila*, when cells along the ventral midline of the embryo constrict their apical surfaces, initiating the formation of a furrow that subsequently internalizes the future mesoderm [24], as shown in Fig. 3(ab). This apical constriction was shown to be driven by pulsed contractions of a *medial* actomyosin network (located on the apical cell surface) that connects to the adherens junction-anchored cortical cytoskeleton. The process has been described as a “ratchet” [29] where medial myosin pulses cause transient constrictions, that are subsequently stabilized by the retracted cytoskeletal cortex.

This phenomenon is readily interpretable in terms of the ATN model. If we assume that the *cortical* myosin concentrations are relatively static over the timescale of medial myosin pulsing, the ATN model predicts that any transient perturbation of mechanical balance due to medial myosin contractions would leave behind an isogonal deformation of the cell array, as it returns to mechanical balance dominated by cortical tensions that remain unchanged. Hence we predict that cell deformation during the early stages of ventral furrow formation should be well described by motion along an isogonal manifold.

However, before testing this prediction, we can test the applicability of the tension balance

hypothesis that underlies the ATN model. While it is not yet possible to measure all internal tensions in a live tissue, the compatibility constraint (3) provides us with an indirect way to evaluate if tension balance may be playing a role in defining geometry of cells. To that end we examine apical snapshots of tissues (e.g. Fig 3a) and calculate χ_α for each cell. We then compare the resultant probability distribution function (PDF) of $\log \chi$ to a “null” distribution constructed from a fictitious cell array with the angles reshuffled while preserving their empirical distribution (see SI for more details). A tension net close to mechanical equilibrium should generate a PDF of χ_α clustering significantly closer to $\chi = 1$ than the null distribution. Fig. 3(c) presents the result of such an analysis for the embryonic mesoderm. Based on the analysis of ~ 5000 cells, we find strong and highly statistically significant (Kolmogorov-Smirnov [25] $p < 10^{-9}$) accumulation of $\log \chi_\alpha$ near zero, consistent with approximate tension balance. (Note that one cannot expect the compatibility constraint to be exact on account of cellular fluctuations and of the noise introduced in image analysis.) This finding is non-trivial as similar analysis of cells in wing imaginal discs [26] reveals no statistically significant tendency towards $\log \chi_\alpha \approx 0$, from which we conclude that tension balance is not a good description of imaginal disc epithelia. (Yet other tissues that we have analyzed (see SI) offer more examples of applicability of the ATN model.)

Returning to the dynamics of VF formation, we used time-lapse microscopy data on the early stage of ventral furrow formation to examine the deformation of cells as a function of time (see SI for details). We found, as shown in Fig. 3(g), that the inferred isogonal modes accounted for about 80% of the total variance of the dynamic vertex displacement field, which clearly indicates that apical deformation of cells during ventral furrow formation is well approximated by an isogonal transformation. Thus, the cell array appears to behave much like a transiently perturbed ATN, flowing along the isogonal manifold which comprises the set of its (mechanical) equilibrium states (see Fig. 2(b)). Consistent with this interpretation, analyzing time-lapse images of Sqh-GFP we found that cortical-myosin levels do not significantly change during this time despite medial-myosin spiking. The results not only suggest that an ATN model is suitable for describing tissue behavior, but also provide a simpler set of degrees of freedom that accurately describe the dynamics. The profile of final isogonal deformation $\{\Theta_\alpha\}$ was found to be approximately parabolic (shown in Fig.

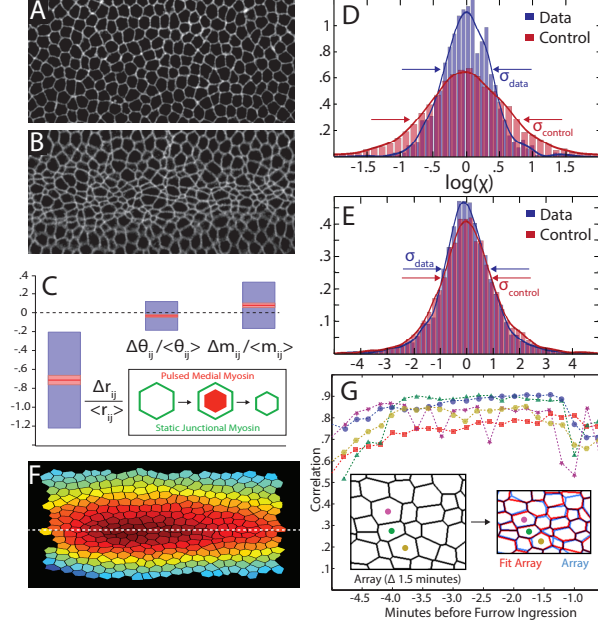


FIG. 3. (a) A ventral view of *Drosophila* embryo at the beginning of VF formation process (top) and (b) 4 minutes later (bottom): note the variability of apical cell area. (c) Observed changes in edge length Δr_{ij} , edge orientation angle $\Delta \theta_{ij}$ and myosin level Δm_{ij} . While edge length shrinks $\sim 75\%$ relative changes in myosin level and edge orientation are considerably smaller. (d-e) Test of compatibility constraint (Eq.5) compares the PDF of the measured $\log \chi$'s (blue) with the control distribution (red) defined by permuting angles. Embryonic mesoderm (d) exhibits a strong tendency towards compatibility ($\log \chi \approx 0$) while epithelium of the third instar imaginal wing disc (e), does not. (f) Spatial profile of the isogonal mode amplitude, $\{\Theta_\alpha\}$ (just before invagination) describes increasing anisotropic compression of cells towards ventral midline. (g) Fraction of deformation $1 - \frac{\langle |\Delta \mathbf{r} - \Delta \mathbf{r}_{iso}|^2 \rangle}{\langle |\Delta \mathbf{r}|^2 \rangle}$ captured by the best-fit isogonal transformation. Each color represents an independent measurement with 200 cells. Inset: a graphical comparison of the fit for a single time-point.

3f), consistent with anisotropic constriction of cells with the long axis oriented along the anterior-posterior direction [24]. This could be patterned via graded medial myosin pulses.

Discussion

ATN model formulated above describes epithelial tissue dynamics in terms of three processes: i) fast relaxation towards mechanical equilibrium dominated by cortical tension; ii) myosin driven rearrangement of cortex on an intermediate time scale and iii) on the slowest timescale, Dynamic Recruitment (or reduction) of myosin driven by the internal rate of strain in the cortex. The 1st two alone would result in a viscoelastic fluid behavior (driven by myosin generated internal forces), Dynamic Recruitment however, dramatically changes the long term behavior so that while being able to flow at short times, ATNs, like solids, can support external stress at long times.

Tension balance imposes a constraint on cell geometry, which we found to be approximately obeyed in some of the epithelial tissues observed during *Drosophila* development. Existence of isogonal “soft modes” predicted by the ATN model was strikingly confirmed by the analysis of cellular deformations in the process of *Drosophila* Ventral Furrow formation, where isogonal modes nicely account for the observed extreme variability of apical area of cells. While these observations confirm the validity of tension balance in describing mechanical equilibrium of epithelial tissue, new experiments will be needed test the Dynamic Recruitment hypothesis, that was introduced to explain how myosin levels at different interfaces can be coordinated to attain equilibrium.

In conclusion, the ATN model describes a very unusual solid - an “Active Solid” - illustrating the wealth of novel physics associated with Living Matter, while providing insight into biological phenomena.

Materials and Methods

The following fly stocks where used for ventral furrow live recordings: Spider GFP [30], sqh-GFP;membrane-mCherry [31]. Embryos where dechoreonated following standard protocols, and mounted in Matek Dishes for imaging. Images where acquired on a Leica SP8 confocal, equipped with a 40x/N.A. 1.1 objective water immersion objective. See SI for details on image analysis and numerical simulation of ATN dynamics.

ACKNOWLEDGMENTS

The authors gratefully acknowledge stimulating discussions with Ken Irvine, Thomas Lecuit, and Eric Wieschaus and would like to thank K. Irvine for sharing the wing imaginal disc data. This work was supported by the NSF PHY-1220616 (BIS) and by the GBMF grant #2919 (BIS/IH).

-
- [1] Bellaiche, Y. Heisenberg, C. (2013). Forces in Tissue Morphogenesis and Patterning. *Cell*, 153(5):948-962
 - [2] Farhadifar, R. Roper, JC. Aigouy, B. Eaton, S. Julicher, F. (2007). The influence of cell mechanics, cell-cell interactions, and the proliferation of epithelial packing. *Current Biology*, 17(24):2095-2104
 - [3] Rauzi, M. Verant, P. Lecuit, T. Lenne, PF. (2008). Nature and anisotropy of cortical forces orienting *Drosophila* tissue morphogenesis. *Nature Cell Bio*, 10:1401-10
 - [4] He B, Doubrovinski K, Polyakov O, Wieschaus E (2014) Apical constriction drives tissue-scale hydrodynamic flow to mediate cell elongation. *Nature* 508: 392-6.
 - [5] Lecuit, T. Lenne, PF. (2007). Cell surface mechanics and the control of cell shape, tissue patterns, and morphogenesis. *Nature MCB*, 8:633-644
 - [6] Nelson, C., Jean, R. Tan, J. Liu, W. Sniadecki, N. Spector, A. Chen, C. et al. (2005). Emergent patterns of growth controlled by multicellular form and mechanics. *PNAS*, 102(33):11594-9
 - [7] Shraiman, B. (2005). Mechanical feedback as a possible regulator of tissue growth. *PNAS*, 102(9):3318-3323
 - [8] Fernandez-Gonzalez, R. Simeos, M. Roper, JC. Eaton, S. Zallen, J. (2009). Myosin II dynamics are regulated by tension in intercalating cells. *Dev. Cell* 17(5):736-43
 - [9] Gilbert S., 2000. *Developmental Biology*. Sinauer Associates, Sunderland.
 - [10] MacKintosh, F.C., Levine, A.J. (2008). Nonequilibrium Mechanics and Dynamics of Motor-Activated Gels. *Phys. Rev. Lett.* 100(1):018104

- [11] Wang N, et al. (2002) Cell prestress. I. Stiffness and prestress are closely associated in adherent contractile cells. *Am J Physiol. Cell Physiol.* 282(3):C606616.
- [12] Salbreux, G. Charras, G. Paluch, E. (2012). Actin cortex mechanics and cellular morphogenesis. *Cell* 22(10):536-545
- [13] Hartsock, A., Nelson, W. J. (2008). Adherens and Tight Junctions: Structure, Function and Connections to the Actin Cytoskeleton. *Biochimica et Biophysica Acta*, 1778(3), 660669.
- [14] Wozniak, M. Chen, C. (2009). Mechanotransduction in development: a growing role for contractility. *Nature MCB* 10:34-43
- [15] Kasza, K. Rowat, A. Liu, J. Angelini, T. Brangwynne, C. Koenderink, G. Weitz, D. (2007). The cell as a material. *Current Opinion in Cell Biology*, 19(1):101-107
- [16] Chiou, K. Hufnagel, L. Shraiman, B. (2012). Mechanical stress inference for two dimensional cell arrays. *PLOS Comp. Bio.*, 8(5)
- [17] Honda, H. (1983). Geometric models for cells in tissues. *International Review for Cytology*, 81:191-248.
- [18] Marchetti, M.C., Joanny, J.F., Ramaswamy, S., Liverpool, T.B., Prost, J. Rao, M. Simha R., Hydrodynamics of soft active matter. *Rev. Mo. Phys.* 85(3):1144-1189
- [19] Clemen, A., et al. (2005). Force-dependent stepping kinetics of myosin-V. *Biophys J.* 88(6):4402-10
- [20] Norstrom, M. Smithback, PA. Rock, R. (2010). Unconventional processive mechanics of non-muscle myosin IIB. *JBC* 285:26326-334
- [21] Kolomeisky, AB. Fisher, M. (2007). Molecular motors: a theorist's perspective. *Chem.*, 58:675-695
- [22] Pouille PA, Ahmadi P, Brunet AC, Farge E. Mechanical signals trigger myosin II redistribution and mesoderm invagination in *Drosophila* embryos. *Sci Signal.* 2009;2:ra16.
- [23] Villain, J. (1980) Two-Dimensional Solids and Their Interaction with Substrates. *Ordering in strongly fluctuating condensed matter systems*, ed. T. Riste (Plenum, New York), p. 221
- [24] Sweeton, D. Parks, S. Costa, M. Wieschaus, E.(1991). Gastrulation in *Drosophila*: the formation of the ventral furrow and posterior midgut invaginations. *Development*, 112(3):775-89

- [25] Massey Jr., F. (1951). The Kolmogorov-Smirnov Test for Goodness of Fit. *Journal of the American Statistical Association*, 46:253, 68-78
- [26] Rauskolb, C, et al. (2014). Cytoskeletal Tension Inhibits Hippo Signaling through an Ajuba-Warts Complex. *Cell*, 158:143-156
- [27] Maxwell J C. (1864). Relaxing in foam, *Phil. Mag.* 27 250
- [28] S. Henkes, C. S. O'Hern, and B. Chakraborty, (2007). *Phys. Rev. Lett.* 99, 038002
- [29] Martin, AC. Kaschube, M. Wieschaus, E. (2009). Pulsed contractions of an actin-myosin network drive apical constriction. *Nature*, 457(7228):495-9
- [30] Morin, X., Daneman, R., Zavortink, M., Chia, W. (2002). A protein trap strategy to detect GFP-tagged proteins expressed in their endogenous loci in *Drosophila*. *PNAS*. 98(26):15050-15055
- [31] Martin, A. C., Gelbart, M., Fernandez-Gonzalez, R., Kaschube, M., Wieschaus, E. (2010). Integration of contractile forces during tissue invagination. *The Journal of Cell Biology* 188, 735749